



## Effect of Anisotropy Structure on Plume Entropy and Reactive Mixing in Helical Flows

Ye, Yu; Chiogna, Gabriele; Lu, Chunhui; Rolle, Massimo

*Published in:*  
Transport in Porous Media

*Link to article, DOI:*  
[10.1007/s11242-017-0964-3](https://doi.org/10.1007/s11242-017-0964-3)

*Publication date:*  
2018

*Document Version*  
Peer reviewed version

[Link back to DTU Orbit](#)

*Citation (APA):*  
Ye, Y., Chiogna, G., Lu, C., & Rolle, M. (2018). Effect of Anisotropy Structure on Plume Entropy and Reactive Mixing in Helical Flows. *Transport in Porous Media*, 121(2), 315-332. DOI: 10.1007/s11242-017-0964-3

---

### General rights

Copyright and moral rights for the publications made accessible in the public portal are retained by the authors and/or other copyright owners and it is a condition of accessing publications that users recognise and abide by the legal requirements associated with these rights.

- Users may download and print one copy of any publication from the public portal for the purpose of private study or research.
- You may not further distribute the material or use it for any profit-making activity or commercial gain
- You may freely distribute the URL identifying the publication in the public portal

If you believe that this document breaches copyright please contact us providing details, and we will remove access to the work immediately and investigate your claim.

This is a Post Print of the article published on line 13<sup>th</sup> November 2017 in Transport in Porous Media. The publishers' version is available at the permanent link: <https://doi.org/10.1007/s11242-017-0964-3>

1  
2 **Effect of Anisotropy Structure on Plume Entropy and Reactive Mixing in**  
3 **Helical Flows**

4  
5  
6 Yu Ye<sup>1</sup>, Gabriele Chiogna<sup>2,3</sup>, Chunhui Lu<sup>1,\*</sup> and Massimo Rolle<sup>4</sup>

7  
8  
9 <sup>1</sup>State Key Laboratory of Hydrology-Water Resources and Hydraulic Engineering, Hohai  
10 University, Nanjing, China

11 <sup>2</sup>Faculty of Civil, Geo and Environmental Engineering, Technical University of Munich,  
12 Arcistraße 21, D-80333 Munich, Germany

13 <sup>3</sup>Institute of Geography, University of Innsbruck, Innrain 52, 6020 Innsbruck, Austria

14 <sup>4</sup>Department of Environmental Engineering, Technical University of Denmark, Miljøvej  
15 Building 115, DK-2800 Lyngby, Denmark

16  
17  
18  
19  
20 \*corresponding author email: [clu@hhu.edu.cn](mailto:clu@hhu.edu.cn)

23 **Abstract**

24 Plume dilution and reactive mixing can be considerably enhanced by helical flows occurring  
25 in three-dimensional anisotropic porous media. In this study, we perform conservative and  
26 reactive transport simulations considering different anisotropy structures of a single inclusion  
27 with the objective of exploring the effect of the inclusion's geometry and orientation on the  
28 patterns of twisted streamlines and on the overall dilution and reaction of solute plumes. We  
29 analyzed one hundred different scenarios by varying key parameters such as the angle of the  
30 anisotropic structures with respect to the average flow velocity, the spacing between  
31 alternated heterogeneous zones of coarse and fine materials, the permeability contrast  
32 between such matrices, and the magnitude of the seepage velocity. Entropy conservation  
33 equations and entropy-based metrics for both conservative and reactive species were adopted  
34 to quantify dilution, reactive mixing and their interactions with the helical flow patterns in the  
35 considered three-dimensional anisotropic setups. The results allowed identifying optimal  
36 anisotropic configurations maximizing mixing and reactions, and yielding enhancement  
37 factors up to 15 times the outcomes of analogous simulations in homogeneous media.  
38 Furthermore, the effects of compound-specific diffusive/dispersive properties of the  
39 transported species were found to be relevant for both plume dilution and reactive mixing in  
40 helical flows.

41

42 *Keywords: anisotropy; helical flow; entropy; dilution; reactive mixing*

43

## 44 **1. Introduction**

45 The interplay between physical mixing processes and (bio)chemical reactions is of crucial  
46 importance for solute transport in natural flows, as well as in engineered systems (e.g.,  
47 Stroock et al. 2002; Weiss and Provenzale 2008). Reaction kinetics are often rate-limiting in  
48 well mixed systems, such as in turbulent flows (e.g., Ottino 1989), whereas mixing controls  
49 chemical and biological reaction rates under poorly mixed conditions. The latter is typically  
50 the case for creeping flows and mixing-controlled reactive transport in porous media (e.g.,  
51 Tartakovsky 2009; Willingham et al. 2008). A number of studies have investigated solute  
52 transport and mixing in porous media setups at different scales: from microfluidic  
53 experiments and pore-scale simulations (e.g., Acharya et al. 2007; Crevacore et al. 2016; de  
54 Anna et al. 2014; Hochstetler et al. 2013; Icardi et al. 2014; Jimenez-Martinez et al. 2015;  
55 Rolle et al. 2012;) to field-scale investigation and modeling studies of transport in aquifer  
56 systems (e.g., Amos et al. 2011; Cirpka et al. 2012; Liedl et al. 2005 and 2011; Prommer et al.  
57 2009; Rolle et al. 2013a; Tuxen et al. 2006; Zarlenga et al. 2013).

58 The heterogeneity of porous formations has been recognized as the key feature for solute  
59 transport and mixing (e.g., Sanchez-Vila et al. 2006). For instance, the role of flow focusing in  
60 high-permeability inclusions and its effect on mixing and reactions in saturated porous media  
61 has been extensively studied in both two-dimensional and three-dimensional experimental and  
62 modeling setups (e.g., Bauer et al. 2009; Castro-Alcala et al. 2012; Cirpka et al. 2011; de  
63 Barros et al. 2015; de Dreuzy et al. 2012; Herrera et al. 2010; Fox et al. 2016; Muniruzzaman  
64 et al. 2014; Werth et al. 2006; Ye et al. 2015a). Compared to heterogeneity, the anisotropy of  
65 porous formations has received considerably less attention in the study of flow and transport  
66 (e.g., Di Dato et al. 2016a and 2016b; Pedretti et al. 2014; Ursino 2004; Zarlenga and Fiori  
67 2015), particularly for the study of mixing and reactive processes. In modeling studies in  
68 three-dimensional anisotropic porous media, Hemker et al. (2004), Hemker and Bakker (2006)

69 and Stauffer (2007) showed the existence of whirling streamlines which can considerably  
70 affect solute transport. The link between complex three-dimensional flow topology in  
71 heterogeneous anisotropic porous media and mixing has been addressed in a few recent  
72 modeling works (Bennet et al. 2017; Chiogna et al. 2014, 2015 and 2016; Cirpka et al. 2015).  
73 Also experimentally, only a limited number of studies have addressed the effects of  
74 anisotropy structures on flow and transport in porous media (e.g., Theis 1967; Ursino 2001;  
75 Ye et al. 2015b and 2016). The work of Ye et al. (2015b) provided first experimental evidence  
76 of helical flow in porous media: helical flow, entailing twisting streamlines, was obtained in a  
77 laboratory flow-through setup packed to obtain a spatially heterogeneous and anisotropic  
78 permeability. The outcomes of such experimental study motivate the model-based  
79 investigation of mixing enhancement in helical flows performed in the current investigation.

80 The objective of this work is to systematically analyze and assess the effects of anisotropy  
81 structures on dilution and reactive mixing enhancement in three-dimensional twisting flows in  
82 porous media. We consider a single macroscopic anisotropic inclusion, obtained with  
83 alternating slices of fine and coarse materials, embedded in a homogeneous porous matrix.  
84 We design twenty-five different configurations by changing the geometry (i.e., the orientation  
85 angle and the width of the alternating slices of low and high hydraulic conductivity) of the  
86 macroscopic anisotropic inclusion resulting in helical flows within the three-dimensional  
87 domain. Simulations of steady-state flow and transport were carried out with a recently  
88 proposed three-dimensional modeling approach to compute twisted flows in anisotropic  
89 media (Cirpka et al. 2015), which was validated with experimental data from high-resolution  
90 flow-through experiments (Ye et al. 2015b). The simulations were performed considering  
91 different seepage velocities, as well as different permeability contrasts between the fine and  
92 coarse porous media. Dilution and reactive mixing enhancement for conservative and  
93 mixing-controlled reactive transport are quantified by considering entropy balances and

94 entropy-based metrics of mixing for both conservative and reactive species. For the reactive  
 95 transport simulations in the different configurations of helical flow, we compute the critical  
 96 dilution index (i.e., the amount of dilution necessary to completely degrade a  
 97 mixing-controlled reactive plume) and we compare the results with the analytical expression  
 98 for a three-dimensional homogeneous porous medium. Finally, we explore the effect of  
 99 compound-specific diffusion in advection-dominated helical flows and its impact on mixing  
 100 of conservative and reactive solute plumes.

## 101 **2. Flow and Transport Modeling**

### 102 **2.1 Governing equations**

103 The governing equation for steady-state flow in porous media is obtained by combining the  
 104 continuity equation with Darcy's law:

$$\nabla \cdot (\mathbf{q}(\mathbf{x})) = \nabla \cdot (-\mathbf{K}(\mathbf{x})\nabla\phi(\mathbf{x})) = 0 \quad (1)$$

105 where  $\mathbf{q}$  [ $\text{LT}^{-1}$ ] is the specific discharge vector,  $\mathbf{K}$  [ $\text{LT}^{-1}$ ] is the hydraulic conductivity tensor,  $\mathbf{x}$   
 106 [ $\text{L}$ ] is the vector of spatial coordinates, and  $\phi$  [ $\text{L}$ ] is the hydraulic head.

107 The advection-dispersion equation describes solute transport in porous media. For  
 108 steady-state reactive transport such equation reads as:

$$\mathbf{v} \cdot \nabla c - \nabla \cdot (\mathbf{D}\nabla c) = r \quad (2)$$

109 where  $\mathbf{v}$  [ $\text{LT}^{-1}$ ] is the seepage velocity vector (i.e.,  $\mathbf{v} = \mathbf{q}/\theta$ ),  $\theta$  [-] is the porosity,  $c$  [ $\text{ML}^{-3}$ ] is the  
 110 concentration,  $\mathbf{D}$  [ $\text{L}^2\text{T}^{-1}$ ] is the hydrodynamic dispersion tensor, and  $r$  [ $\text{ML}^{-3}\text{T}^{-1}$ ] is the reaction  
 111 rate which equals to zero for conservative solute transport. For steady-state transport of  
 112 continuously emitted plumes, the transverse component of the dispersion tensor is of key  
 113 importance (Cirpka et al. 2011). In this work we describe the transverse dispersion coefficient,  
 114  $D_t$  [ $\text{L}^2\text{T}^{-1}$ ], with the non-linear, compound-specific parameterization proposed by Chiogna et

115 al. (2010) i.e.,  $D_t = D_p + D_{aq} \left( \frac{Pe^2}{Pe + 2 + 4\delta^2} \right)^\beta$ , in which  $D_p$  [ $L^2T^{-1}$ ] is the pore diffusion  
 116 coefficient,  $Pe = vd/D_{aq}$  [-] is the grain Péclet number,  $v$  [ $LT^{-1}$ ] is the magnitude of the seepage  
 117 velocity,  $d$  [L] is the grain diameter,  $D_{aq}$  [ $L^2T^{-1}$ ] is the aqueous diffusion coefficient,  $\delta$  [-] is  
 118 the ratio between the length of a pore channel and its hydraulic radius, and  $\beta$  [-] is an  
 119 empirical exponent that accounts for the degree of incomplete mixing within the pore  
 120 channels. Values of  $\delta=5.37$  and  $\beta=0.5$  were taken from the study of Ye et al. (2015c), which  
 121 compiled experimental data on transverse dispersion from a number of two-dimensional and  
 122 fully three-dimensional flow-through experiments in porous media with different grain sizes.

123 In the reactive transport scenarios, we considered a simple instantaneous bimolecular reaction  
 124 (i.e.,  $f_aA + f_bB \rightarrow f_cC$ ), such that the reaction is completely mixing-controlled. Here  $f_a$ ,  $f_b$  and  $f_c$   
 125 are the stoichiometric coefficients of the reaction, which were set to unity in this study.  
 126 Species  $A$  represents the plume of continuously emitted contaminant, whereas species  $B$  is a  
 127 reactant presented in the ambient water. Assuming the same diffusive properties for the two  
 128 reactants, a virtual conservative compound  $X$  [-], denoted as mixing ratio, can be used to  
 129 describe the reactive transport problem (Cirpka and Valocchi 2007).  $X$  represents the  
 130 volumetric ratio of the source-related solution in the mixture with the ambient solution. The  
 131 critical mixing ratio,  $X_{crit}$  [-], is the value of  $X$  at which the concentrations of both reactants

132 are zero.  $X_{crit}$  is defined as  $X_{crit} = \frac{f_a c_B^{amb}}{f_b c_B^{amb} + f_a c_A^{in}}$ , where  $c_B^{amb}$  [ $ML^{-3}$ ] is the concentration of

133 species  $B$  in the ambient water and  $c_A^{in}$  [ $ML^{-3}$ ] is the concentration of species  $A$  at the inlet  
 134 source. The concentrations of the different reactive species can be obtained from the  
 135 distribution of the conservative mixing ratio. For instance, the concentration of reactant  $A$  (i.e.  
 136  $c_A$ ) and product  $C$  (i.e.  $c_C$ ), can be computed as:

$$c_A = \begin{cases} Xc_A^{in} - \frac{f_a}{f_b}(1-X)c_B^{amb} & X \geq X_{crit} \\ 0 & X < X_{crit} \end{cases} \quad (3)$$

$$c_C = \begin{cases} \frac{f_c}{f_b}(1-X)c_B^{amb} & X \geq X_{crit} \\ \frac{f_c}{f_a}Xc_A^{in} & X < X_{crit} \end{cases} \quad (4)$$

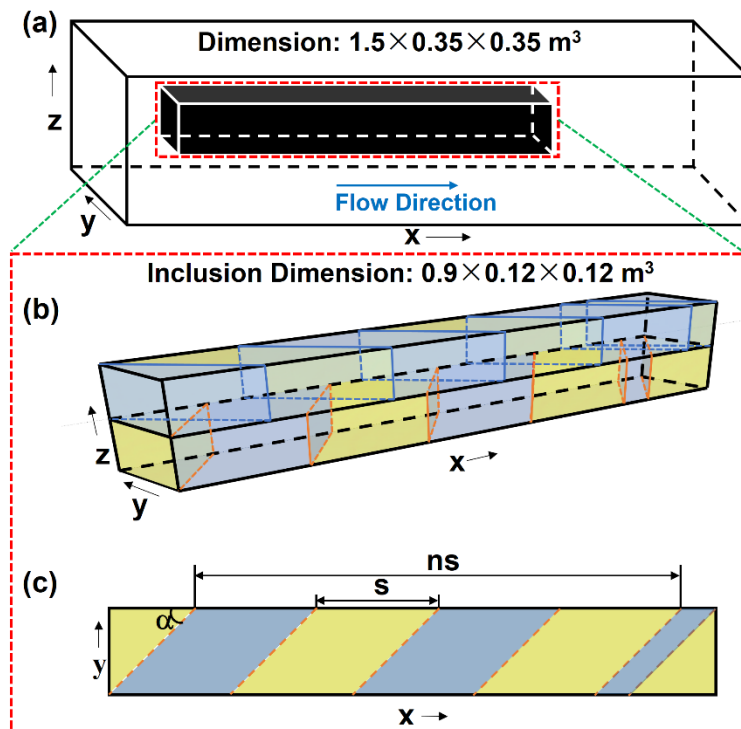
## 137 2.2 Numerical model

138 The flow-through domain has dimensions of 1.5 m × 0.35 m × 0.35 m (length × width ×  
139 height) and represents a hypothetical intermediate scale fully three-dimensional laboratory  
140 setup. The domain was discretized into 183750 cells, with the cell size of 0.01 m in each  
141 direction. The flow-through system was described as a confined aquifer. Flow was solved  
142 applying a cell-centered finite volume method. Constant flow boundary conditions were set at  
143 the inlet and at the outlet of the flow-through domain. Injection and extraction of solutions at  
144 the inlet and outlet of the flow-through setup was simulated with 49 cells representing  
145 injection and extraction ports. No-flow was imposed at the other boundaries of the system. A  
146 particle tracking algorithm based on Pollock's scheme (1988), was used to compute the  
147 streamlines, using 60025 particles released at the inlet. Steady-state transport was simulated  
148 with the method recently proposed by Cirpka et al. (2015), solving for advective transport  
149 along the streamlines and dispersive mass exchange in the transverse direction. At each cross  
150 section perpendicular to the longitudinal direction  $x$ , transverse dispersion was computed by  
151 Finite Volume approach on Voronoi polygons for each streamline. To simulate continuous  
152 injection, a constant mass flux was set at the inlet whereas no flux conditions were set at the  
153 top, side, and bottom boundaries. The plumes of conservative tracer or reactant A were  
154 injected at the central inlet port, whereas pure water or a solution containing reactant B was  
155 injected from the surrounding inlet ports.

156 As shown in Figure 1a, a heterogeneous anisotropic inclusion was inserted in the otherwise



157 homogeneous matrix. The hydraulic conductivity of the matrix was  $2.5 \times 10^{-3}$  m/s. The  
 158 inclusion had a dimension of  $0.90 \text{ m} \times 0.12 \text{ m} \times 0.12 \text{ m}$ . The inclusion consisted of two layers  
 159 with alternating angled slices of coarse and fine porous media (Figure 1b). In order to achieve  
 160 macroscopic anisotropy, the direction of the angled slices were opposite between the two  
 161 layers. Figure 1c shows a 2-D view of the bottom layer: the angle between the slices and the  
 162 flow direction is indicated by  $\alpha$  [°], whereas  $s$  [L] represents the spacing of the slices. The fine  
 163 material of the inclusion (i.e., indicated by a blue color in Figures 1b and 1c) had the same  
 164 permeability of the matrix, whereas the coarse material (i.e., yellow in Figures 1b and 1c) had  
 165 a higher hydraulic conductivity of  $3.06 \times 10^{-2}$  m/s or  $3.03 \times 10^{-1}$  m/s, resulting in a permeability  
 166 contrast ( $k_{contr}$  [-]) of 12.5 or 121, respectively. The grain diameters of the materials were  
 167 directly related to their permeability according to the relation of Hazen (1892), i.e.,  $K=(Cd)^2$ ,  
 168 where  $C=100 \text{ m}^{-0.5} \text{ s}^{-0.5}$ . Porosity was set as 0.4 for both the fine and coarse porous media.



169

170 **Fig. 1** Geometry of the 3-D setup: a) overview of the domain; b) anisotropy structure of the  
 171 inclusion; c) top view of the bottom layer of the inclusion, the top layer has an identical

172 structure but an opposite direction of the slices. Yellow color: high permeability medium;  
173 Blue color: low permeability medium;  $\alpha$ : angle between the slice and the main flow direction;  
174  $s$ : distance between the slices.

175 Different anisotropy structures were designed by varying  $\alpha$ ,  $s$ , and  $k_{contr}$ , but maintaining  
176 identical total volumes of high- and low-permeability materials, as well as the position of the  
177 inclusion, which was aligned with the central injection port and started at 0.20 m in the  $x$   
178 direction. Fifty different heterogeneous anisotropic structures were constructed with the  
179 parameters values of  $\alpha$ ,  $s$ , and  $k_{contr}$  listed in Table 1. Notice, that when  $\alpha$  equals to 0 or 90  
180 degrees, the heterogeneous inclusion becomes macroscopically isotropic.

181 Table 1 Values of  $\alpha$ ,  $s$  and  $k_{contr}$  used for the construction of the inclusion.

Parameter	Value
$\alpha$	0°, 11.25°, 22.5°, 45°, 90°
$s$	0.03 m, 0.05 m, 0.10 m, 0.15 m, 0.25 m
$k_{contr}$	12.25, 121

182

183 The simulations were performed at average seepage velocities of 3 m/d and 0.3 m/d, thus  
184 resulting in 100 scenarios. For conservative transport a solute with the same aqueous  
185 diffusivity as fluorescein ( $D_{aq}=0.48\times 10^{-9}$  m<sup>2</sup>/s) was used. In selected cases, focusing on the  
186 compound-specific dispersion effects in helical flows, multitracer transport simulations were  
187 run considering an additional solute with the diffusivity of oxygen ( $D_{aq}=1.97\times 10^{-9}$  m<sup>2</sup>/s).  
188 Species with the aqueous diffusivities values of fluorescein and oxygen were also considered  
189 for the evaluation of the compound-specific behavior during mixing-controlled reactive  
190 transport.

### 191 2.3 Entropy balance and metrics of mixing

192 Approaches based on the Shannon entropy have been developed and applied in different fields  
 193 of geosciences and engineering (e.g., Bianchi and Pedretti 2017; Cabeza and Karunanithi  
 194 2008; Kitanidis 1994; Singh 1997). In particular, for solute transport in porous media such  
 195 approaches are powerful tools to quantify the dilution of solute plumes (e.g., Aquino and  
 196 Bolster 2017; Beckie 1998; de Barros et al. 2015; Dentz et al. 2011; Kapoor and Kitanidis  
 197 1996; Kitanidis 1994; Paster et al. 2015; Rolle and Kitanidis 2014; Thierrin and Kitanidis  
 198 1994; Ursino 2001). Considering a flux-related framework, the transport equation of the  
 199 entropy density of a conservative solute reads as (Chiogna et al. 2011):

$$\mathbf{v} \cdot \nabla(-p_Q \ln p_Q) - \nabla \cdot (\mathbf{D} \nabla(-p_Q \ln p_Q)) = \frac{1}{p_Q} \nabla p_Q^T \mathbf{D} \nabla p_Q \quad (5)$$

200 where  $p_Q = \frac{c}{\int_{\Omega} c q_x dA}$  [TL<sup>-3</sup>] is the flux-weighted probability density function of the solute  
 201 mass, and  $q_x$  [LT<sup>-1</sup>] is the specific-discharge in  $x$  direction. The term on the right hand side of  
 202 Eq. 5 represents a positive source of entropy due to dilution.

203 It is also interesting to consider the governing transport equation for the entropy density of a  
 204 reactive species, which can be written as (Chiogna et al. 2012):

$$\mathbf{v} \cdot \nabla(-p_Q \ln p_Q) - \nabla \cdot (\mathbf{D} \nabla(-p_Q \ln p_Q)) = -(1 + \ln p_Q) r^* + \frac{1}{p_Q} \nabla p_Q^T \mathbf{D} \nabla p_Q \quad (6)$$

205 where the reactive term  $r^*$  is defined as  $r^* = \left( \frac{\partial p_Q}{\partial c} - \frac{1}{r} \frac{\partial^2 p_Q}{\partial c^2} \nabla c^T \mathbf{D} \nabla c \right) r$ .

206 Comparing Eq. 5 and Eq. 6 it can be noticed that an additional term on the right hand side  
 207 appears for the reactive transport case. This term represents the contribution of reactive  
 208 mixing, which can act as a sink in the entropy transport. The balance between entropy sources  
 209 and sinks provides relevant insights on the interplay between dilution and reactive processes.

210 The flux-related dilution index,  $E_Q$ , is an entropy-based metric of mixing that has been

211 proposed to quantify dilution of conservative plumes continuously emitted from a  
 212 contaminant source (Rolle et al. 2009). This quantity represents an effective volumetric  
 213 discharge that transports the solute mass flux at a given cross-section along the main flow  
 214 direction and has been applied as metric of mixing in experimental and modeling studies (e.g.,  
 215 Ballarini et al. 2013; Cirpka et al. 2015; Rolle et al. 2013b). Mathematically, the flux-related  
 216 dilution index is defined as the exponential of the Shannon entropy, in analogy to the  
 217 volumetric dilution index introduced by Kitanidis (1994) for a solute slug:

$$E_Q(x) = \exp\left(-\int_{\Omega} (p_Q(x, y, z) \ln p_Q(x, y, z)) q_x(x, y, z) dA\right) \quad (7)$$

218 where  $\Omega$  is the cross-section perpendicular to the longitudinal direction  $x$ .

219 The rate of increase of the natural logarithm of flux-related dilution index corresponds to the  
 220 rate of increase of the entropy in the mean flow direction  $x$  (i.e., integration of Eq. 5 over  $\Omega$   
 221 for a conservative solute) and reads as (Chiogna et al. 2011, 2012):

$$\frac{d \ln(E_Q)}{dx} = \int_{\Omega} \frac{1}{p_Q} \nabla p_Q^T \mathbf{D} \nabla p_Q d\Omega \quad (8)$$

222 The flux-related dilution index and its rate of increase can also be computed for a reactant. In  
 223 this case,  $E_Q(x)$  is no more a monotonically increasing function with the travel distance but its  
 224 trend is determined by the balance between the entropy source and sink terms due to dilution  
 225 and reactive processes (Eq. 6). For reactive transport, an additional metric of mixing that is  
 226 considered in this study is the critical dilution index (i.e.,  $CDI$  [ $L^3T^{-1}$ ]). The  $CDI$  is defined as  
 227 the mixing amount required for the complete degradation of a reactive plume (i.e., species  $A$   
 228 in our study) undergoing an instantaneous bimolecular reaction (Chiogna et al. 2011). The  
 229 value of the  $CDI$  is equal to the flux-related dilution index of a conservative plume at the  
 230 distance  $L$  from the source (i.e.,  $CDI = E_Q(L)$ ), where  $L$  [ $L$ ] is the length of the reactive plume.  
 231 Analytical expressions can be derived for the  $CDI$  in homogeneous domains. A simple  
 232 first-order approximation for the  $CDI$  in a three-dimensional system was derived in a previous

233 study (Ye et al. 2016) and reads as:

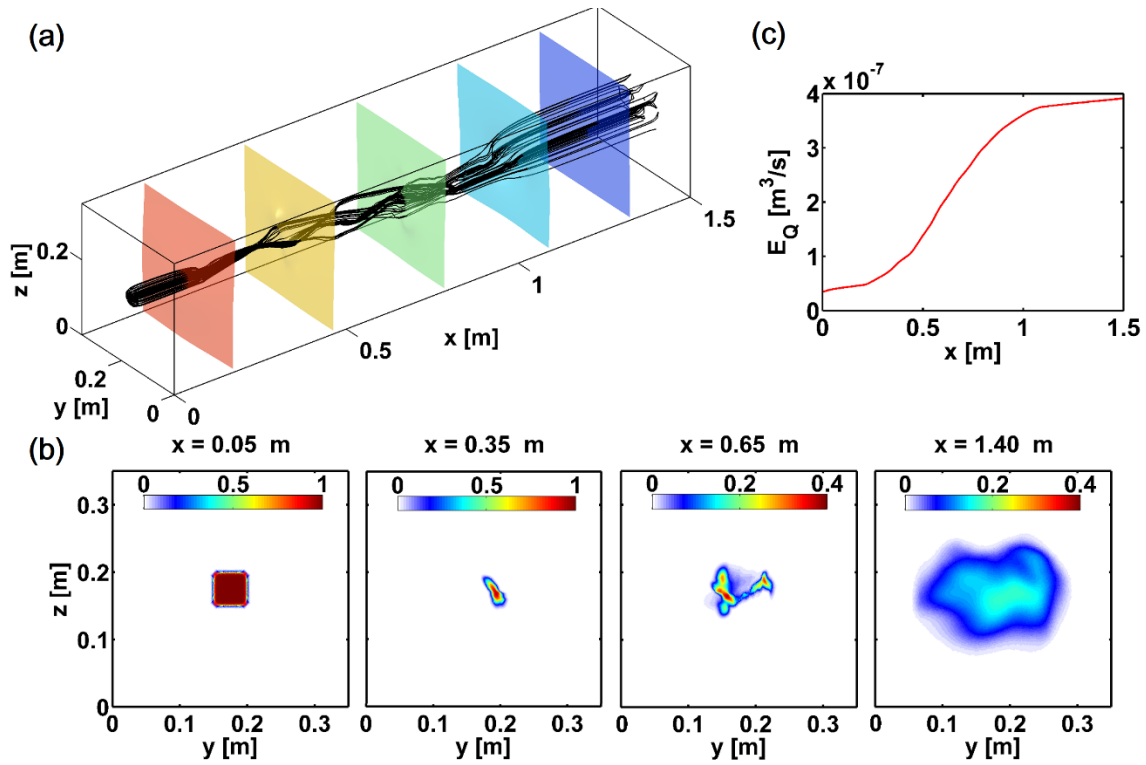
$$CDI_{theor} = \frac{E_Q(0)}{X_{crit}} \exp(1) \quad (9)$$

234

## 235 **3. Results and Discussion**

### 236 **3.1 Conservative transport**

237 Different patterns of twisting streamlines caused by the different anisotropic structures were  
238 observed in the particle-tracking simulations. Furthermore, the outcomes of the conservative  
239 transport modeling resulted in plumes with reduced peak concentration and a monotonic  
240 entropy increase along the main flow direction. As an illustrative example, Figure 2 shows the  
241 results for the setup with  $\alpha$ ,  $s$ ,  $k_{contr}$  and  $v$  equal to 22.5°, 0.10 m, 12.25, and 3 m/d,  
242 respectively. Streamlines (49 black lines in Figure 2a) traced from the central inlet port are  
243 straight until they reach the anisotropic inclusion. At the inclusion, the streamlines are focused  
244 due to the presence of the high-permeability medium and follow a twisting pattern induced by  
245 the geometric structure of the inclusion. The complex three-dimensional flow due to the  
246 macroscopic anisotropic inclusion has a remarkable impact on solute transport. In fact the  
247 plume, continuously injected from the central inlet port, is strongly deformed, stretched and  
248 squeezed as can be observed in two-dimensional concentration distribution maps at different  
249 cross sections (Figure 2b). The streamlines twisting can also cause the plume to split into  
250 different parts (e.g.,  $x=0.65$  m), each with its own peak concentration. The twisting flow  
251 behavior deforms the material surface of the plume and favors the contact and the  
252 diffusive/dispersive mass exchange between the plume and the surrounding clean water. This  
253 leads to an enhancement of plume dilution that, as quantified by the flux-related dilution  
254 index, is particularly pronounced at the location of the macroscopic anisotropic inclusion  
255 (Figure 2c).

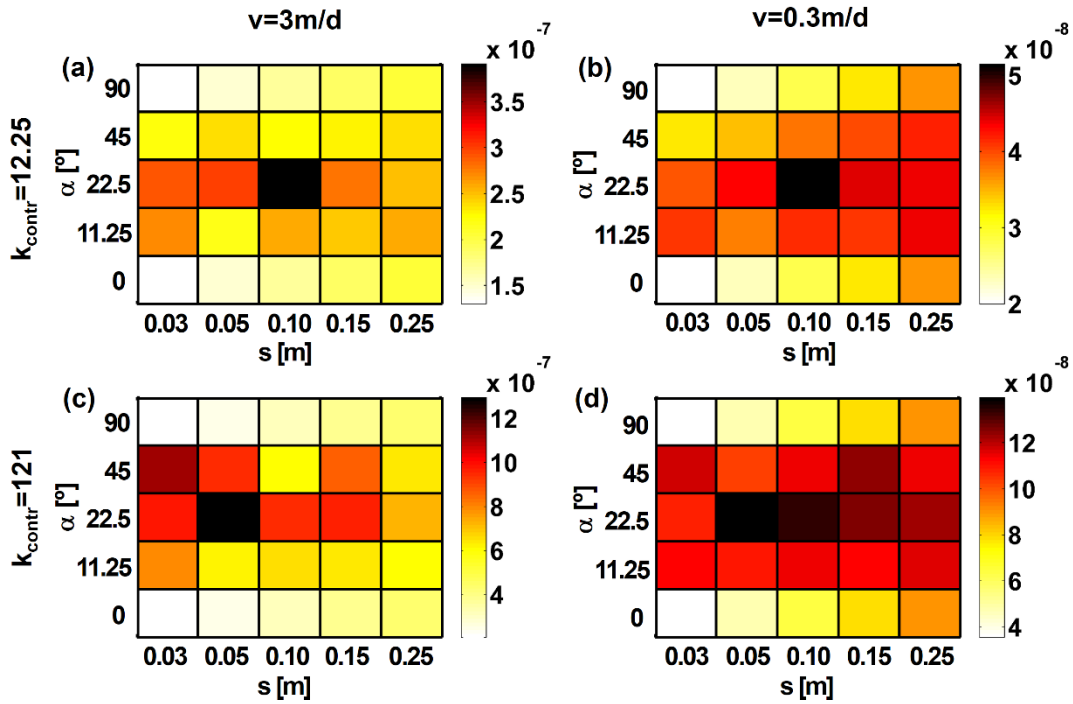


256

257 **Fig. 2** Flow and transport in a heterogeneous anisotropic setup ( $s=0.10$  m,  $\alpha=22.5^\circ$ ,  
 258  $k_{contr}=12.25$ ,  $v=3$  m/d): a) Streamlines traced from the central inlet show a twisting pattern;  
 259 black lines: streamlines; colored surfaces: isosurfaces of hydraulic head; b) Concentration  
 260 distribution at different cross-sections; c) Flux-related dilution index along the travel distance.

261 Plume dilution was computed for all 100 conservative transport scenarios simulated, based on  
 262 the parameters listed in Table 1, at seepage velocities of 3 and 0.3 m/d. Figure 3 shows the  
 263 computed  $E_Q$  values at the outlet of the flow-through domain. The results are visualized as  
 264 four matrices, corresponding to the two seepage velocities and permeability contrasts. Each  
 265 matrix contains the outcomes of simulations in which the angle of the slices (along the  
 266 columns) and their distances (along the rows) were systematically changed. The difference of  
 267 the anisotropy structure has a strong impact on plume dilution and leads to different values of  
 268 flux-related dilution index at the outlet. Notice that, for the setups with an angle of  $90^\circ$  or  $0^\circ$ ,  
 269 the streamlines do not twist, the material surface of the plume is not significantly deformed,  
 270 and dilution is smaller compared to the anisotropic setups. The results show that, for a

271 specified seepage velocity and permeability contrast, there is an optimal configuration of the  
 272 anisotropy structure that maximizes the dilution enhancement. For instance, in the setups with  
 273 a permeability contrast of 12.25, the maximum dilution is achieved at  $\alpha=22.5^\circ$  and  $s=0.10$  m.  
 274 In contrast, the maximum dilution is reached for the configuration of  $\alpha=22.5^\circ$  and  $s=0.05$  m  
 275 for the permeability contrast of 121.



276

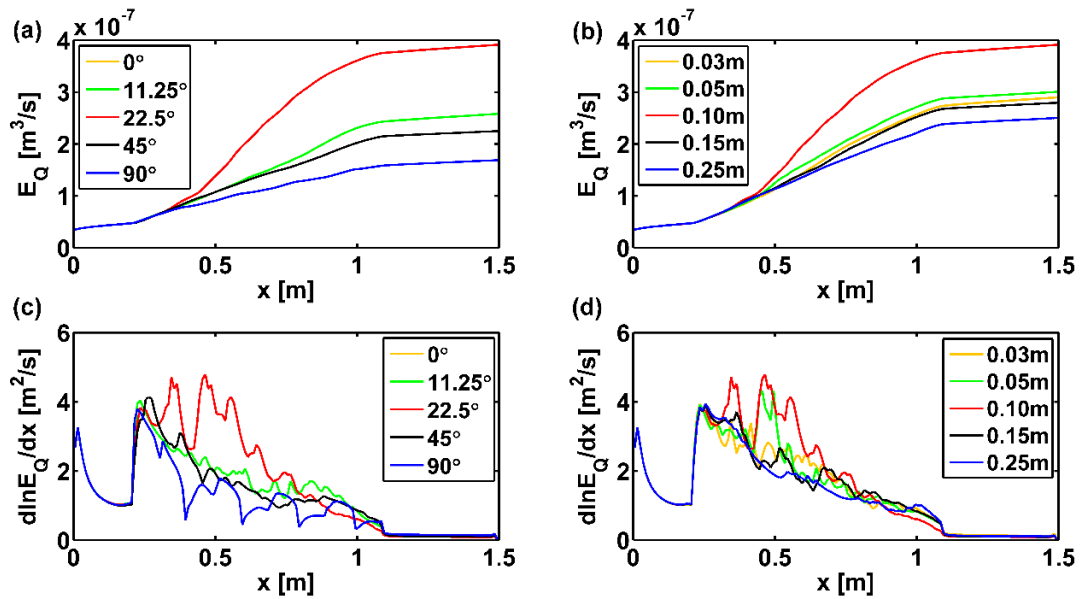
277 **Fig. 3** Flux-related dilution index at the outlet of the domain for different heterogeneous  
 278 anisotropic setups: a)  $v=3$  m/d,  $k_{contr}=12.25$ ; b)  $v=0.3$  m/d,  $k_{contr}=12.25$ ; c)  $v=3$  m/d,  $k_{contr}=121$ ;  
 279 d)  $v=0.3$  m/d;  $k_{contr}=121$ .

280 Both the magnitude of the seepage velocity and the permeability contrast affect plume  
 281 dilution. As shown in Figure 3, for a given permeability contrast, dilution is larger at 3 m/d  
 282 than at 0.3 m/d, since transverse dispersion, which controls plume dilution, depends on the  
 283 flow velocity. Similarly, for a given value of seepage velocity, a larger permeability contrast  
 284 enhances diffusive/dispersive mass exchange between the plume and the surrounding solution,  
 285 thus resulting in stronger plume dilution.

286 To illustrate the development of the plume entropy along the travel distance, we consider  
287 selected scenarios with flow velocity of 3 m/d and  $k_{contr}$  of 12.25. The cases correspond to the  
288 row ( $\alpha=22.5^\circ$ ) and the column ( $s=0.10$  m) in Figure 3a, containing the scenario with  
289 maximum plume dilution. Figure 4 shows the flux-related dilution index and its rate of  
290 increase along the flow direction for the selected cases. The monotonic increase of the plume  
291 entropy is strongly affected by the geometry (both angle and spacing) of the anisotropic  
292 inclusion. For instance, Figure 4a shows that the flux-related dilution index in the scenario  
293 with the heterogeneous slices are inclined at  $22.5^\circ$  is more than double with respect to the  $90^\circ$   
294 case. The rate of increase of the flux-related dilution index (Eq. 8) is also illustrative of the  
295 complex mixing dynamics induced by the twisting flows in the different anisotropic setups  
296 (Figure 4c and 4d). After an initial decrease and stabilization of  $d\ln E_Q/dx$  in the homogeneous  
297 matrix due to flow defocusing effect from the inlet port, an interesting pattern with significant  
298 increase of plume dilution is apparent as the plume reaches the anisotropic inclusion. Several  
299 peaks of dilution enhancement are related to the geometry of the heterogeneous anisotropic  
300 inclusion and to the helical pattern of the streamlines. For instance, in the case of different  
301 angles (Figure 4c), plume focusing and twisting yields more pronounced peaks of  $d\ln E_Q/dx$   
302 resulting in stronger dilution enhancement. Such number of peaks that can be considered “hot  
303 spots of mixing”, associated with the occurrence of plume focusing and twisting within the  
304 anisotropic inclusion also depends on the spacing between the alternating slices of fine and  
305 coarse material (Figure 4d). The rate of increase of the dilution index is positive in the whole  
306 domain since its expression corresponds to the source term in the entropy density balance for  
307 a conservative solute (Eq. 5). The overall trend shows progressively lower rates of increase  
308 for  $E_Q$  within the anisotropic inclusion. Such behavior can be explained by the stronger  
309 concentration gradients as the plume reaches the inclusion and their attenuation further  
310 downstream as the plume becomes progressively more diluted. In fact, as expressed by Eq. 8,  
311 the rate of increase of the flux-related dilution index depends on the transverse dispersion



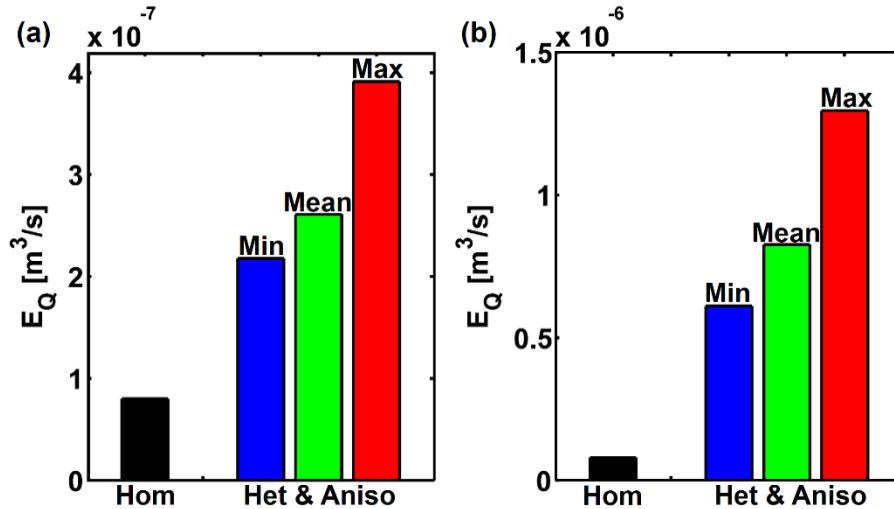
312 coefficient and on the solute concentration gradients.



313

314 **Fig. 4** Flux-related dilution index along the travel distance for selected setups with  $v=3$  m/d,  
 315  $k_{contr}=12.25$ : a)  $s=0.10$  m; b)  $\alpha=22.5^\circ$ . Rate of increase of the flux-related dilution index for  
 316 the same scenarios: c)  $s=0.10$  m; d)  $\alpha=22.5^\circ$ .

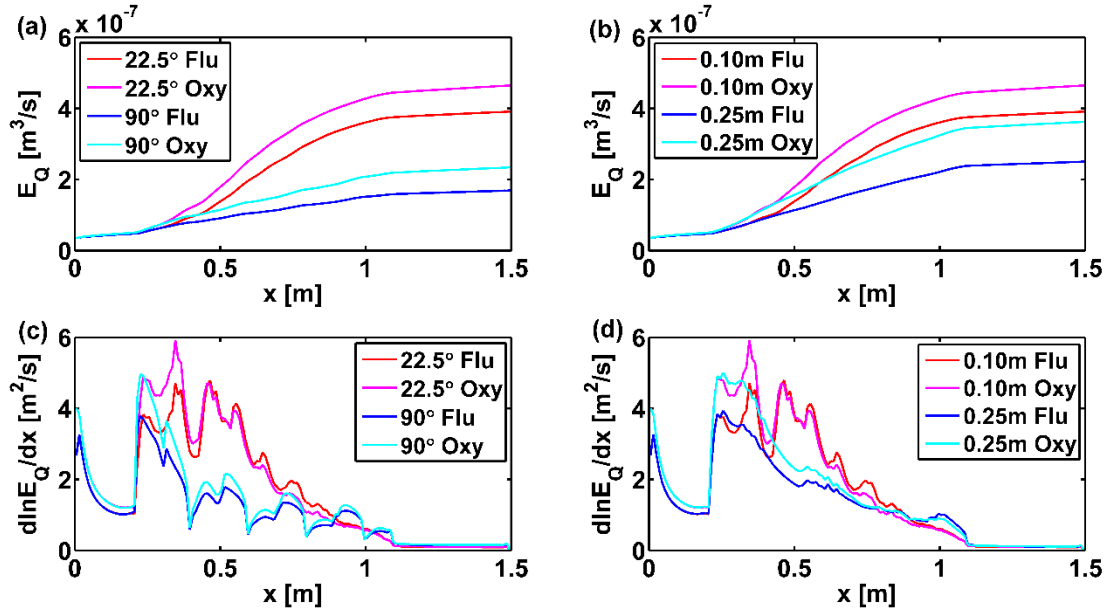
317 Figures 5a and 5b show the dilution at the outlet for the setups at an average flow velocity of  
 318 3 m/d and considering a permeability contrast of 12.25 and 121, respectively. The colored  
 319 bars represent the minimum, average and maximum dilution achieved in the anisotropic  
 320 setups, while the black bar is the dilution obtained in a corresponding homogeneous isotropic  
 321 system. The average value of  $E_Q$  obtained in the heterogeneous anisotropic setups are 225%  
 322 and 930% larger for the cases with a permeability contrast of 12.25 and 121, respectively,  
 323 compared to the homogeneous setup. The maximum relative differences of  $E_Q$  (i.e., relative  
 324 difference between the red and black bars) are 388% and 1516% for the permeability contrast  
 325 of 12.25 and 121, respectively. Even the minimum relative differences of  $E_Q$  (i.e., relative  
 326 difference between the blue and black bars) show a significant dilution enhancement (172%  
 327 and 662% for the cases with a permeability contrast of 12.25 and 121, respectively) in the  
 328 presence of a heterogeneous anisotropic inclusion.



329

330 **Fig. 5** Flux-related dilution index at the outlet for the cases: a)  $v=3$  m/d,  $k_{contr}=12.25$  (25  
 331 scenarios); b)  $v=3$  m/d,  $k_{contr}=121$  (25 scenarios). Hom: Homogeneous setup; Het&Aniso:  
 332 Heterogeneous anisotropic setup with angled slices (Min: Minimal value; Mean: Mean value;  
 333 Max: Maximum value).

334 To investigate compound-specific effects in helical flows, multitracer conservative transport  
 335 simulations were performed considering an additional tracer with the diffusivity of oxygen.  
 336 Such simulations were run for the cases of minimal and maximum entropy illustrated in  
 337 Figure 4. Figure 6 shows the flux-related dilution index and the spatial derivative of its natural  
 338 logarithm along the flow direction for both solutes. In Figures 6a and 6b, oxygen (i.e., with  
 339 higher diffusivity) is more diluted than fluorescein (i.e., with lower diffusivity), which is  
 340 consistent with the effect shown in isotropic porous media. The entropy of the solutes  
 341 increases with a similar pattern in a specific anisotropy configuration (see Figures 6c and 6d).  
 342 The difference of dilution between the two solutes depends on the specific value of  $\ln E_Q/dx$ ,  
 343 particularly at the beginning of the inclusion where the plumes focus and twist within the  
 344 heterogeneous anisotropic structure and the compound-specific diffusivities control lateral  
 345 mass exchange.



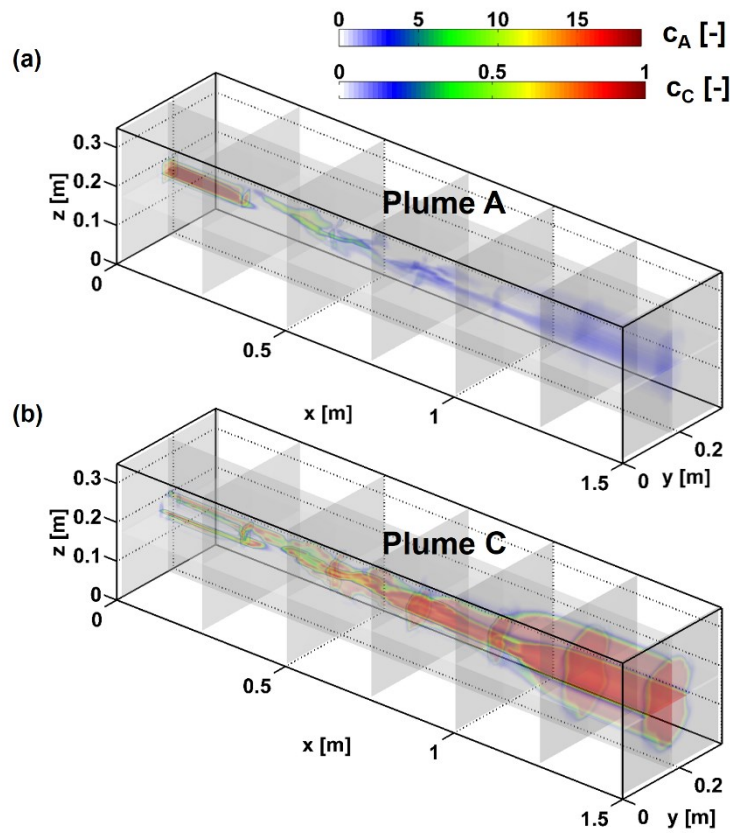
346

347 **Fig. 6** Flux-related dilution index along the travel distance using two tracers with aqueous  
 348 diffusivity of fluorescein and oxygen: a)  $s=0.10$  m; b)  $\alpha=22.5^\circ$ . Rate of increase of the  
 349 flux-related dilution index for the same scenarios: c)  $s=0.10$  m; d)  $\alpha=22.5^\circ$ .

### 350 3.2 Reactive transport

351 Reactive transport was investigated considering the same scenarios analyzed for conservative  
 352 transport. Figure 7 shows an example of mixing-controlled reactive transport in which the  
 353 plumes of the reactant  $A$  and product  $C$  are visualized in a heterogeneous anisotropic domain.  
 354 The simulation was performed with a critical mixing ratio of 0.05, considering a source  
 355 concentration of reactant  $A$  ( $c_A^{in}$ ) of 19 and an initial concentration of reactant  $B$  ( $c_B^{amb}$ ) of 1  
 356 in the ambient water. The reactant  $A$  is not significantly consumed in the initial portion of the  
 357 domain (i.e., at  $x < 0.2$  m). When the plumes reach the inclusion, the concentration of  $A$   
 358 reduces drastically and the plume surfaces of both  $A$  and  $C$  are deformed due to the twisting  
 359 flow pattern. After the inclusion (i.e., at  $x > 1.1$  m), the flow in the matrix becomes uniform  
 360 again and also the reactive plumes have a more regular shape, as shown by the concentration  
 361 distributions in the down gradient cross-sectional planes (i.e., last two  $y$ - $z$  cross sections in

362 Figures 7a and 7b).

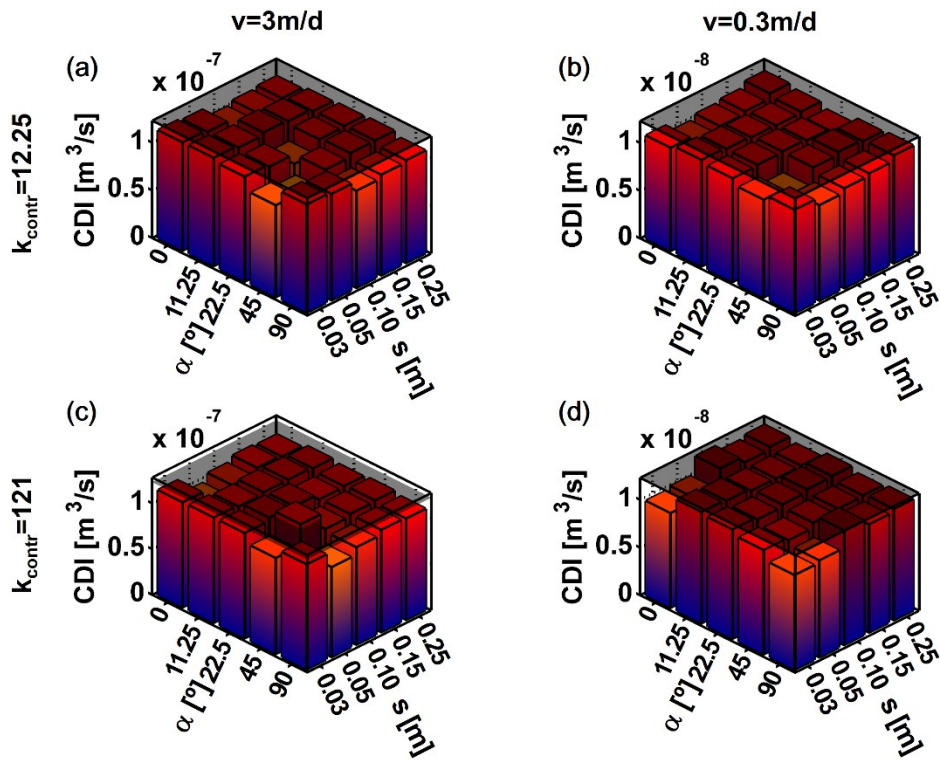


363

364 **Fig. 7** Plumes computed for a mixing-controlled reactive transport simulation in a  
365 heterogeneous anisotropic domain: a) reactant *A*; b) product *C*.

366 Also for mixing-controlled reactive transport we considered 100 scenarios based on the  
367 geometric parameters and permeability contrasts of the anisotropic inclusion listed in Table 1,  
368 as well as the seepage velocities of 3 and 0.3 m/d. With the aim of analyzing the critical  
369 dilution index (*CDI*) in the different anisotropic setups, we considered both reactants with the  
370 aqueous diffusivity of fluorescein and with dimensionless inlet concentration of 0.3 and 1 for  
371 reactant *A* and reactant *B*, respectively. This corresponds to a critical mixing ratio of 0.77 and  
372 results in steady-state plume lengths for the reactant *A* ending within the considered  
373 three-dimensional domain. The values of critical dilution index were calculated based on the  
374 flux-related dilution index of a conservative tracer at the end of the reactive plume. The  
375 results are shown in Figure 8 for the considered seepage velocities and permeability contrasts.

376 The critical dilution index is very similar in all scenarios (4% relative difference) showing  
 377 that also in the case of complex three-dimensional flow in anisotropic setup the value of the  
 378 critical dilution index does not depend significantly on the heterogeneity and anisotropy of the  
 379 system. The outcomes of the numerical simulations were also compared with the theoretical  
 380 value of the critical dilution index,  $CDI_{theor}$  (Eq. 9). The comparison yields satisfactory results  
 381 (average relative difference of 10%), although the first order approximation expressed by Eq.  
 382 9 (gray surface in Figure 8) tends to slightly overestimate the mixing needed for the complete  
 383 degradation of a reactive plume compared to the values computed with the numerical model.  
 384 Such discrepancy stems from the assumption of sufficiently long plumes (i.e., small  $X_{crit}$ ) in  
 385 the derivation of the analytical expression (Ye et al. 2016).

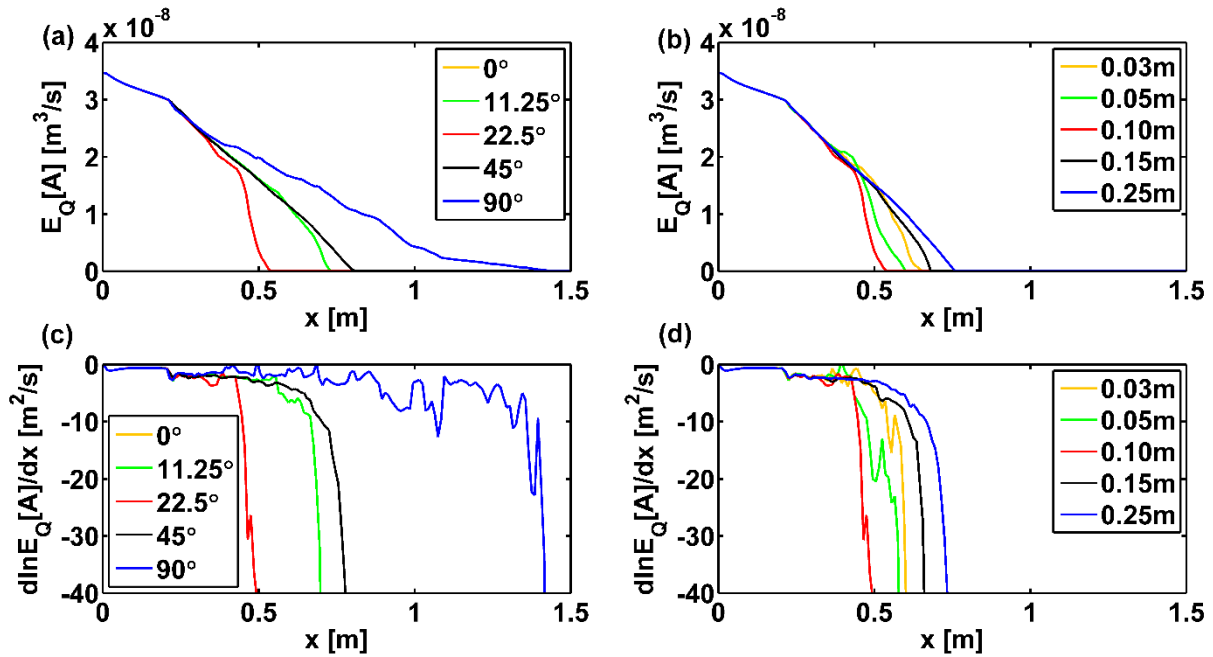


386

387 **Fig. 8** Critical dilution index for the different heterogeneous anisotropic setups: a)  $v=3$  m/d,  
 388  $k_{contr}=12.25$ ; b)  $v=0.3$  m/d,  $k_{contr}=12.25$ ; c)  $v=3$  m/d,  $k_{contr}=121$ ; d)  $v=0.3$  m/d;  $k_{contr}=121$ . Gray  
 389 surface: theoretical critical dilution index.

390 Figure 9 shows the flux-related dilution index of reactant  $A$  (indicated as  $E_Q[A]$ ) and its

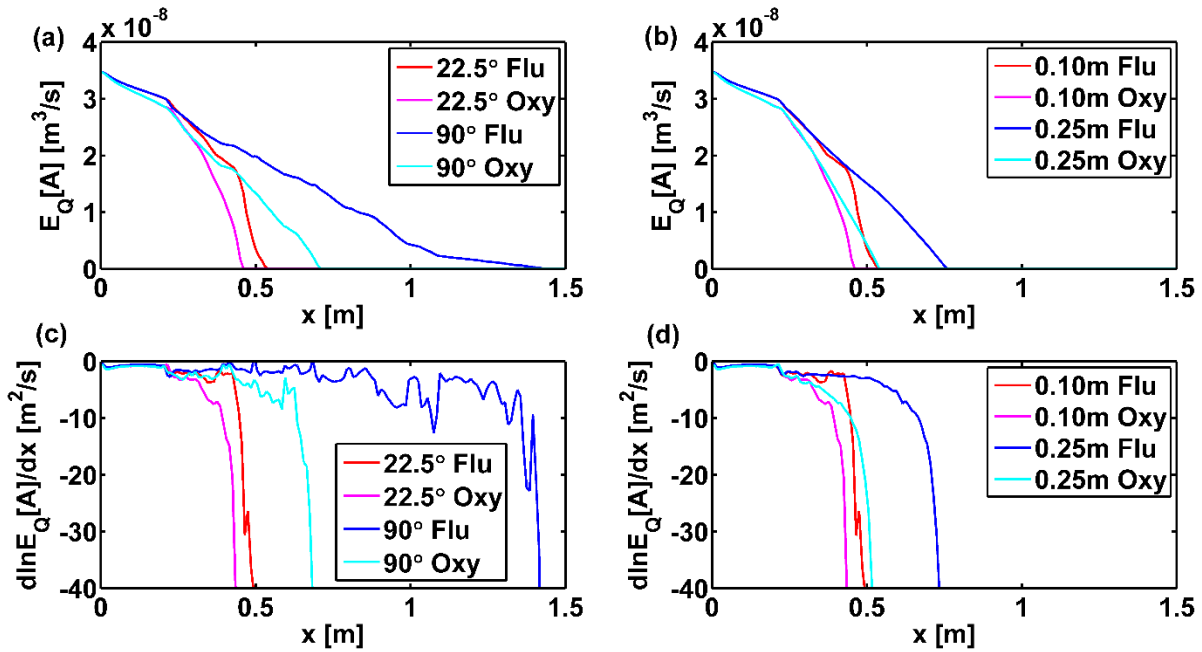
391 spatial derivative in the same setups selected for the illustration of plume dilution in the case  
 392 of conservative transport (Figure 4). Here  $c_A^{in}$  was set to 0.9 and  $c_B^{amb}$  was kept as 1,  
 393 yielding  $X_{crit}=0.53$ . Since the reaction is instantaneous and the source concentration of  $A$  is  
 394 low, the flux-related dilution index is decreasing in all setups indicating that the reactive sink  
 395 term dominates the entropy density balance for reactive transport (Eq. 6). This is also  
 396 substantiated by the negative values of  $d\ln E_Q[A]/dx$  (Figures 9c and 9d). For  
 397 mixing-controlled reactive transport, a stronger dilution of conservative solute, caused by the  
 398 focusing and twisting flow (Figure 4), corresponds to a faster consumption of reactant  $A$  in  
 399 Figure 9. For instance, in the case of  $\alpha=22.5^\circ$ , the plume of reactant  $A$  is almost three times  
 400 shorter than the analogous case with  $\alpha=90^\circ$  (Figure 9a). In fact, local enhancements of  
 401 transverse mixing directly imply reaction enhancements and shorter plumes of reactant  $A$ .



402  
 403 **Fig. 9** Flux-related dilution index of reactant  $A$  along the travel distance for selected setups  
 404 with  $v=3$  m/d,  $k_{contr}=12.25$ : a)  $s=0.10$  m; b)  $\alpha=22.5^\circ$ . Rate of increase of the flux-related  
 405 dilution index for reactant  $A$  in the same scenarios: c)  $s=0.10$  m; d)  $\alpha=22.5^\circ$ .

406 Compound-specific effects were also investigated for mixing-controlled reactive transport.

407 We considered the scenarios examined above for the conservative tracer (Figure 6) and  
 408 computed reactive transport considering reactive species both with aqueous diffusivity of  
 409 fluorescein and oxygen. Figure 10 shows the results illustrated as flux-related dilution index  
 410 of reactant  $A$ . In case of higher diffusivity, the reactant plume is shorter. Such  
 411 compound-specific effect is more important for the cases with less pronounced mixing  
 412 enhancement and less important when mixing enhancement is maximized. This behavior can  
 413 be attributed to more important kinematic effects and shorter residence times before complete  
 414 plume degradation in the scenarios in which the anisotropic inclusion causes a more  
 415 significant mixing enhancement (i.e., cases for  $\alpha=22.5^\circ$ ).



416

417 **Fig. 10** Compound-specific effects on the flux-related dilution index of reactant  $A$  along the  
 418 travel distance. The simulations were performed with reactants with aqueous diffusivities of  
 419 fluorescein and oxygen: a) Scenarios with  $s=0.10$  m and b)  $\alpha=22.5^\circ$ . Rate of increase of the  
 420 flux-related dilution index for reactant  $A$ : c)  $s=0.10$  m; d)  $\alpha=22.5^\circ$ .

#### 421 4. Summary and Conclusions

422 In this work we have investigated the effect of anisotropy structures on conservative and

423 mixing-controlled reactive transport in porous media. We have performed a large number of  
424 numerical simulations in fully three-dimensional heterogeneous anisotropic setups. In such  
425 setups, the geometrical configuration of macroscopic anisotropic inclusions cause complex  
426 flow fields, entailing twisting streamlines. Our results show that the anisotropy-induced  
427 secondary motion and the flow focusing due to permeability contrast have a major impact on  
428 plume dilution and reaction. By constructing 25 different anisotropy structures we could  
429 systematically investigate the effect of key geometrical parameters such as the angle  
430 orientation of alternating slices of fine and coarse materials with respect to the average flow  
431 velocity, as well as their spacing. The outcome of the analysis allowed identifying optimal  
432 anisotropic configurations maximizing mixing and reactions, and yielding substantial mixing  
433 enhancement compared to analogous simulations in homogeneous media. Entropy balance  
434 equations and entropy-based metrics of mixing provided an adequate framework to quantify  
435 the enhancement of dilution in the conservative transport scenarios and the enhancement of  
436 reactive mixing when reaction between two initially segregated reactants was considered. The  
437 analysis based on the concept of Shannon entropy also allowed us to establish a link between  
438 the complex flow field and the key phenomena of flow-focusing and streamlines twisting with  
439 the local increase of mixing. This was apparent for both conservative and reactive transport  
440 scenarios. For conservative transport the interpretation is more straightforward since the  
441 plume entropy monotonically increases along the travel distance; whereas for reactive  
442 transport the entropy balance depends on the relative impact of a source term due to physical  
443 dispersive mixing and a sink term entailing the effects of the chemical reaction.

444 This study contributes to improve the understanding of solute transport in complex fully  
445 three-dimensional flow in porous media. 3-D features such as helical patterns of streamlines  
446 have a strong impact on transport and mixing but cannot be observed in more conventional  
447 two-dimensional setups. The outcomes of this work have implications for applications in both



448 natural and engineered systems. For instance, sedimentological observation of aquifer  
449 outcrops (e.g., Heinz et al. 2003) often shows more complex heterogeneous anisotropic  
450 patterns than those considered in common realizations of heterogeneous media for simulation  
451 of flow and contaminant transport in groundwater. In fact the latter are often based on  
452 two-dimensional representations and typically do not consider the effect of anisotropy.  
453 Moreover, in engineering applications it may be of interest to design devices, such as porous  
454 media static mixers, which can induce mixing and reaction between two initially segregated  
455 fluids and/or solutes. To this end, the outcomes of this study show the importance of the  
456 geometry and anisotropic structures, as well as the possibility to find configurations allowing  
457 maximizing plume dilution and reactive mixing. Further investigation is also necessary to  
458 develop upscaling rules for conservative and mixing-controlled reactive transport in complex  
459 flow fields. To this end, numerical flow and transport simulations in larger scales  
460 heterogeneous anisotropic domains could help finding effective upscaled parameters and  
461 contribute to fill the gap between laboratory and field observations.

462

## 463 **Acknowledgments**

464 This study was supported by the National Natural Science Foundation of China (51709085).  
465 Y. Ye acknowledges the support of “The Fundamental Research Funds for the Central  
466 Universities” (2017B00214) and a project funded by the Priority Academic Program  
467 Development of Jiangsu Higher Education Institutions. G. Chiogna acknowledges the support  
468 of the Stiftungsfonds für Umweltökonomie und Nachhaltigkeit GmbH (SUN). C. Lu  
469 acknowledges the support of the National Natural Science Foundation of China (51679067)  
470 and the “111 Project” (B17015), Ministry of Education and State Administration of Foreign  
471 Experts Affairs, P. R. China. M. Rolle acknowledges the support of the Danish Council for  
472 Independent Research (DFF) and of the Sino-Danish Center. The authors would like to thank

473 Prof. O.A. Cirpka for discussion on helical flows and for providing an earlier version of the  
474 code that has been used in this study.

475

## 476 **References**

- 477 Acharya, R.C., Valocchi, A.J., Werth, C.J., Willingham, T.W.: Pore-scale simulation of  
478 dispersion and reaction along a transverse mixing zone in two-dimensional porous media.  
479 *Water Resour. Res.* **43**, W10435 (2007)
- 480 Amos, R.T., Berkins, B.A., Delin, G.N., Cozzarelli, I.M., Blowes, D.W., Kirshtein, J.D.:  
481 Methane oxidation in a crude oil contaminated aquifer: delineation of aerobic reactions  
482 at the plume fringes. *J. Contam. Hydrol.* **125**, 13-25 (2011)
- 483 Aquino, T., Bolster, D.: Localized point mixing rate potential in heterogeneous velocity fields.  
484 *Trans. Porous Medi.* **119**, 391-402 (2017)
- 485 Ballarini, E., Bauer, S., Eberhardt, C., Beyer, C.: Evaluation of the role of heterogeneities on  
486 transverse mixing in bench-scale tank experiments by numerical modeling. *Ground*  
487 *Water* **52**, 368-377 (2013)
- 488 Bauer, R.D., Rolle, M., Bauer, S., Eberhardt, C., Grathwohl, P., Kolditz, O., Meckenstock,  
489 R.U., Griebler, C.: Enhanced biodegradation by hydraulic heterogeneities in petroleum  
490 hydrocarbon plumes. *J. Contam. Hydrol.* **105**, 56-68 (2009)
- 491 Beckie, R. D.: Analysis of scale effects in large-scale solute transport models. In: Sposito, G.  
492 (eds.) *Scale Dependence and Scale Invariance in Hydrology*, pp. 314-334. Cambridge  
493 Univ. Press, New York (1998)
- 494 Bennett, J.P., Haslauer, C.P., Cirpka, O.A.: The impact of sedimentary anisotropy on solute  
495 mixing in stacked scour-pool structures. *Water Resour. Res.* **53**, 2813-2832 (2017)
- 496 Bianchi, M., Pedretti, D.: Geological entropy and solute transport in heterogeneous porous  
497 media, *Water Resour. Res.*, **53**, 4691–4708 (2017)
- 498 Cabezas, H., Karunanithi, A.T.: Fisher information, entropy, and the second and third laws of  
499 thermodynamics. *Ind. Eng. Chem. Res.* **47**, 5243–5249 (2008)
- 500 Castro-Alcala, E., Fernandez-Garcia, D., Carrera, J., Bolster, D.: Visualization of mixing  
501 processes in a heterogeneous sand box aquifer. *Environ. Sci. Technol.* **46**, 3228-3235  
502 (2012)
- 503 Chiogna, G., Eberhardt, C., Grathwohl, P., Cirpka, O.A., Rolle, M.: Evidence of

504 compound-dependent hydrodynamic and mechanical transverse dispersion by multitracer  
505 laboratory experiments. *Environ. Sci. Technol.* **44**, 688-693 (2010)

506 Chiogna, G., Cirpka, O.A., Grathwohl, P., Rolle, M.: Transverse mixing of conservative and  
507 reactive tracers in porous media: Quantification through the concepts of flux-related and  
508 critical dilution indices. *Water Resour. Res.* **47**, W02505 (2011)

509 Chiogna, G., Hochstetler, D.L., Bellin, A., Kitanidis, P.K., Rolle, M.: Mixing, entropy and  
510 reactive solute transport. *Geophys. Res. Lett.* **39**, L20405 (2012)

511 Chiogna, G., Rolle, M., Alberto, B., Cirpka, O.A.: Helicity and flow topology in  
512 three-dimensional anisotropic porous media. *Adv. Water Resour.* **73**, 134-143 (2014)

513 Chiogna, G., Cirpka, O.A., Rolle, M., Alberto, B.: Helical flow in three-dimensional  
514 nonstationary anisotropic heterogeneous porous media. *Water Resour. Res.* **51**, 261-280  
515 (2015)

516 Chiogna, G., Cirpka, O.A., Herrera, P.A.: Helical flow and transient solute dilution in porous  
517 media. *Transp. Porous Med.* **111**, 591-603 (2016)

518 Cirpka, O.A., Valocchi A.J.: Two-dimensional concentration distribution for  
519 mixing-controlled bioreactive transport in steady state. *Adv. Water Resour.* **30**,  
520 1668-1679 (2007)

521 Cirpka, O.A., de Barros, F.P.J., Chiogna, G., Rolle, M., Nowak, W.: Stochastic flux-related  
522 analysis of transverse mixing in two-dimensional heterogeneous porous media. *Water*  
523 *Resour. Res.* **47**, W06515 (2011)

524 Cirpka, O.A., Rolle, M., Chiogna, G., de Barros, F.P., Nowak, W.: Stochastic evaluation of  
525 mixing-controlled steady-state plume lengths in two-dimensional heterogeneous domains.  
526 *J. Contam. Hydrol.* **138-139**, 22-39 (2012)

527 Cirpka, O.A., Chiogna, G., Rolle, M., Bellin, A.: Transverse mixing in three-dimensional  
528 non-stationary anisotropic heterogeneous porous media. *Water Resour. Res.* **51**, 241-260  
529 (2015)

530 Crevacore, E., Tosco, T., Sethi, R., Boccardo, G., Marchisio, D.L.: Recirculation zones induce  
531 non-Fickian transport in three-dimensional periodic porous media. *Phys. Rev. E* **94**,  
532 053118 (2016)

533 de Anna, P., Jimenez-Martinez, J., Tabuteau, H., Turuban, R., Le Borgne, T., Derrien, M.,  
534 Meheust, Y.: Mixing and reaction kinetics in porous media: an experimental pore scale  
535 quantification. *Environ. Sci. Technol.* **48**, 508-516 (2014)

536 de Barros, F.P.J., Fiori, A., Boso, F., Bellin, A.: A theoretical framework for modeling dilution  
537 enhancement of non-reactive solutes in heterogeneous porous media. *J. Contam. Hydrol.*

538           **175**, 72-83 (2015)

539 de Dreuzy, J.R., Carrera, J., Dentz, M., Le Borgne, T.: Time evolution of mixing in  
540 heterogeneous porous media. *Water Resour. Res.* **48**, W06511 (2012)

541 Dentz, M., Le Borgne, T., Englert, A., Bijeljic, B.: Mixing, spreading and reaction in  
542 heterogeneous media: A brief review. *J. Contam. Hydrol.* **120-121**, 1-17 (2011)

543 Di Dato, M., de Barros, F.P.J., Fiori, A., Bellin, A.: Effects of the hydraulic conductivity  
544 microstructure on macrodispersivity. *Water Resour. Res.* **52**, 6818-6832 (2016a)

545 Di Dato, M., Fiori, A., Chiogna, G., de Barros, F.P.J., Bellin, A.: Impact of the spatial  
546 structure of the hydraulic conductivity field on vorticity in three-dimensional flows. *Proc.*  
547 *R. Soc. A.* **472**, The Royal Society (2016b)

548 Fox, D.T., Guo, L., Fujita, Y., Huang, H., Redden, G.: Experimental and numerical analysis of  
549 parallel reactant flow and transverse mixing with mineral precipitation in homogeneous  
550 and heterogeenosu porous media. *Transp. Porous Med.* **111**, 605-626 (2016)

551 Hazen, A.: Some physical properties of sands and gravels with special reference to their use in  
552 filtration. *Ann. Rep. State Board of Health Mass* **24**, 541-556 (1892)

553 Hemker, K., van den Berg, E., Bakker, M.: Ground water whirls. *Ground Water* **42**, 234-242  
554 (2004)

555 Hemker, K., Baker, M.: Analytical solutions for whirling groundwater flow in  
556 two-dimensional heterogeneous anisotropic aquifers. *Water Resour. Res.* **42**, W12419  
557 (2006)

558 Heinz, J., Kleineidam, S., Teutsch, G., Aigner, T.: Heterogeneity patterns of quaternary  
559 glaciofluvial gravel bodies (SW-Germany): Application to hydrogeology. *Sediment. Geol.*  
560 **158**, 1-23 (2003).

561 Herrera, P.A., Valocchi, A.J., Beckie, R.D.: A multidimensional streamline-based method to  
562 simulate reactive solute transport in heterogeneous porous media. *Adv. Water Resour.* **33**,  
563 711-727 (2010)

564 Hochstetler, D.L., Rolle, M., Chiogna, G., Haberer, C.M., Grathwohl, P., Kitanidis, P.K.:  
565 Effects of compound-specific transverse mixing on steady-state reactive plumes: Insights  
566 from pore-scale simulations and Darcy-scaly experiments. *Adv. Water Resour.* **54**, 1-10  
567 (2013)

568 Icardi, M., Boccardo, G., Marchisio, D., Tosco, T., Sethi, R.: Pore-scale simulation of fluid  
569 flow and solute dispersion in three-dimensional porous media. *Phys. Rev. E* **90**, 013032  
570 (2014)

571 Jiménez-Martínez, J., de Anna, P., Tabuteau, H., Turuban, R., Le Borgne, T., Méheust, Y.:

572 Pore-scale mechanisms for the enhancement of mixing in unsaturated porous media and  
573 implications for chemical reactions. *Geophys. Res. Lett.* **42**, 5316-5324 (2015)

574 Kapoor, V., Kitanidis, P.K.: Concentration fluctuations and dilution in two-dimensionally  
575 periodic heterogeneous porous media. *Transp. Porous Med.* **22**, 91-119 (1996)

576 Kitanidis, P.K.: The concept of dilution index. *Water Resour. Res.* **30**, 2011-2026 (1994)

577 Liedl, R., Valocchi, A.J., Dietrich, P., Grathwohl, P.: Finiteness of steady state plumes. *Water*  
578 *Resour. Res.* **41**, 3923-3929 (2005)

579 Liedl, R., Yadav, P.K., Dietrich, P.: Length of 3-D mixing-controlled plumes for a fully  
580 penetrating contaminant source with finite width. *Water Resour. Res.* **47**, W08602 (2011)

581 Muniruzzaman, M., Haberer, C.H., Grathwohl, P., Rolle, M.: Multicomponent ionic  
582 dispersion during transport of electrolytes in heterogeneous porous media: Experiments  
583 and model-based interpretation. *Geochim. Cosmochim. Acta* **141**, 656-669 (2014)

584 Ottino, J.M.: *The Kinematics of Mixing*. Cambridge University, Cambridge (1989)

585 Paster, A., Aquino, T., Bolster, D.: Incomplete mixing and reactions in laminar shear flow.  
586 *Phys. Rev. E* **92**, 012922 (2015)

587 Pedretti, D., Fernández-García, Sánchez-Vila, X., Bolster, D., Benson, D.A.: Apparent  
588 directional mass-transfer capacity coefficients in three-dimensional anisotropic  
589 heterogeneous aquifers under radical convergent transport. *Water Resour. Res.* **50**,  
590 1205-1224 (2014)

591 Pollock, D.W.: Semianalytical computation of path lines for finite-difference models. *Ground*  
592 *Water* **26**, 743-750 (1988)

593 Prommer, H., Anneser, B., Rolle, M., Einsiedl, F., Griebler, C.: Biogeochemical and isotopic  
594 gradients in a BTEX/PAH contaminant plume: Model-based interpretation of a  
595 high-resolution field data set. *Environ. Sci. Technol.* **43**, 8206-8212 (2009)

596 Rolle, M., Eberhardt, C., Chiogna, G., Cirpka, O.A., Grathwohl, P.: Enhancement of dilution  
597 and transverse reactive mixing in porous media: experiments and model-based  
598 interpretation. *J. Contam. Hydrol.* **110**, 130-142 (2009)

599 Rolle, M., Hochstetler, D., Chiogna, G., Kitanidis, P.K., Grathwohl, P.: Experimental  
600 investigation and pore-scale modeling interpretation of compound-specific transverse  
601 dispersion in porous media. *Transp. Porous Med.* **93**, 347-362 (2012)

602 Rolle, M., Chiogna, G., Hochstetler, D.L., Kitanidis, P.: On the importance of diffusion and  
603 compound-specific mixing for groundwater transport: An investigation from pore to field  
604 scale. *J. Contam. Hydrol.* **153**, 51-68 (2013a)

605 Rolle, M., Muniruzzaman, M., Haberer, C.M., Grathwohl, P.: Coulombic effects in

606 advection-dominated transport of electrolytes in porous media: Multicomponent ionic  
607 dispersion. *Geochim. Cosmochim. Acta* **120**, 195-205 (2013b)

608 Rolle, M., Kitanidis, P.K.: Effects of compound-specific dilution on transient transport and  
609 solute breakthrough: A pore-scale analysis. *Adv. Water Resour.* **71**, 186-199 (2014)

610 Sanchez-Vila, X., Guadagnini, A., Carrera, J.: Representative hydraulic conductivities in  
611 saturated groundwater flow. *Rev. Geophys.* **44**, 535-540 (2006)

612 Staufer, F.: Impact of highly permeable sediment units with inclined bedding on solute  
613 transport in aquifers. *Adv. Water Resour.* **30**, 2194-2201 (2007)

614 Singh, V.P.: The use of entropy on hydrology and water resources. *Hydrol. Process* **11**,  
615 587-626 (1997)

616 Stroock, A.D., Dertinger, S.K.W., Ajdari, A., Mezić, I., Stone, H.A., Whitesides, G.M.:  
617 Chaotic mixer for microchannels. *Science* **295**, 647-651 (2002)

618 Tartakovsky, A.M., Tartakovsky, G.D., Scheibe, T.D.: Effects of incomplete mixing on  
619 multicomponent reactive transport. *Adv. Water Resour.* **32**, 1674-1679 (2009)

620 Theis, C.V.: Aquifers and models. In: *Symposium on Ground-Water Hydrology*, San  
621 Francisco, California, 1967. *Am. Water Resour. Assoc. Proc. Ser.* **4**, 138-148 (1967)

622 Thierrin, J., Kitanidis, P.K.: Solute dilution at the Borden and Cape Cod groundwater tracer  
623 tests. *Water Resour. Res.* **30**, 2883-2890 (1994)

624 Tuxen, N., Albrechtsen, H., Bjerg, P.L.: Identification of a reactive degradation zone at a  
625 landfill leachate plume fringe using high resolution sampling and incubation techniques.  
626 *J. Contam. Hydrol.* **85**, 179-194 (2006)

627 Ursino, N., Gimmi, T., Flühler, H.: Combined effects of heterogeneity, anisotropy, and  
628 saturation on steady state flow and transport: A laboratory sand tank experiment. *Water*  
629 *Resour. Res.* **37**, 201-208 (2001)

630 Ursino, N.: Modeling media with oriented structures. *Transp. Porous Med.* **55**, 137-151  
631 (2004)

632 Weiss, J.B., Provenzale, A.: *Transport and mixing in geophysical flows*. Springer, Berlin  
633 (2008)

634 Werth, C.J., Cirpka, O.A., Grathwohl, P.: Enhanced mixing and reaction through flow  
635 focusing in heterogeneous porous media. *Water Resour. Res.* **42**, W12414 (2006)

636 Willingham, T.W., Werth, C.J., Valocchi, A.J.: Evaluation of the effects of porous media  
637 structure on mixing-controlled reactions using pore-scale modeling and micromodel  
638 experiments. *Environ. Sci. Technol.* **42**, 3185-3193 (2008)

639 Ye, Y., Chiogna, G., Cirpka, O.A., Grathwohl, P., Rolle, M.: Enhancement of plume dilution

640 in two-dimensional and three-dimensional porous media by flow focusing in  
641 high-permeability inclusions, *Water Resour. Res.* **51**, 5582-5602 (2015a)

642 Ye, Y., Chiogna, G., Cirpka, O.A., Grathwohl, P., Rolle M.: Experimental evidence of helical  
643 flow in porous media. *Phys. Rev. Lett.* **115**, 194502 (2015b)

644 Ye, Y., Chiogna, G., Cirpka, O.A., Grathwohl, P., Rolle M.: Experimental investigation of  
645 compound-specific dilution of solute plumes in saturated porous media: 2-D vs. 3-D  
646 flow-through systems. *J. Contam. Hydrol.* **172**, 33-47 (2015c)

647 Ye, Y., Chiogna, G., Cirpka, O.A., Grathwohl, P., Rolle, M.: Experimental investigation of  
648 transverse mixing in porous media under helical flow conditions. *Phys. Rev. E* **94**,  
649 013113 (2016)

650 Zarlenga, A., Janković, I., Fiori, A.: Advective transport in heterogeneous formations: The  
651 impact of spatial anisotropy on the breakthrough curve. *Trans. Porous Med.* **96**, 295-304  
652 (2013)

653 Zarlenga, A., Fiori, A.: Advective transport through three-dimensional anisotropic formations  
654 of bimodal hydraulic conductivity. *Trans. Porous Med.* **107**, 573-593 (2015)